Biochimica et Biophysica Acta 1857 (2016) 1290–1299

Contents lists available at ScienceDirect

Biochimica et Biophysica Acta

journal homepage: www.elsevier.com/locate/bbabio

Probing of protein localization and shuttling in mitochondrial microcompartments by FLIM with sub-diffraction resolution☆

Anna-Carina Söhnel [a,c], Wladislaw Kohl [a], Ingo Gregor [b], Jörg Enderlein [b], Bettina Rieger [a,c], Karin B. Busch [a,c,*]

[a] Mitochondrial Dynamics, School of Biology, University of Osnabrück, D-49076 Osnabrück, Germany
[b] Physics Department III, University of Göttingen, D-37077 Göttingen, Germany
[c] Institute of Molecular Cell Biology, Department of Biology, Westfälische Wilhelms-Universität Münster, D-48149 Münster, Germany

ARTICLE INFO

Article history:
Received 17 December 2015
Received in revised form 17 March 2016
Accepted 18 March 2016
Available online 23 March 2016

Keywords:
Mitochondrial compartments
Fluorescence lifetime imaging microscopy
Nano-environment sensing
Protein localization
Live cell imaging
Sub-diffraction localization analysis

ABSTRACT

The cell is metabolically highly compartmentalized. Especially, mitochondria host many vital reactions in their different microcompartments. However, due to their small size, these microcompartments are not accessible by conventional microscopy. Here, we demonstrate that time-correlated single-photon counting (TCSPC) fluorescence lifetime-imaging microscopy (FLIM) classifies not only mitochondria, but different microcompartments inside mitochondria. Sensor proteins in the matrix had a different lifetime than probes at membrane proteins. Localization in the outer and inner mitochondrial membrane could be distinguished by significant differences in the lifetime. The method was sensitive enough to monitor shifts in protein location within mitochondrial microcompartments. Macromolecular crowding induced by changes in the protein content significantly affected the lifetime, while oxidizing conditions or physiological pH changes had only marginal effects. We suggest that FLIM is a versatile and completive method to monitor spatiotemporal events in mitochondria. The sensitivity in the time domain allows for gaining substantial information about sub-mitochondrial localization overcoming diffraction limitation. This article is part of a Special Issue entitled 'EBEC 2016: 19th European Bioenergetics Conference, Riva del Garda, Italy, July 2-6, 2016', edited by Prof. Paolo Bernardi.

1. Introduction

Metabolism in cells is compartmented to exclude interference between opposing metabolic pathways. It also allows for the maintenance of different physico-chemical environments. Mitochondria are organelles that *per se* provide numerous microcompartments for different reactions by two membranes enclosing two aqueous compartments, the intermembrane space (IMS) and the matrix [1]. The outer mitochondrial membrane (OMM) has a case structure and harbors proteins of the protein import machinery, tethering enzymes for interaction with other organelles and diverse carriers and pores. The inner mitochondrial membrane (IMM) is folded manifold into cristae providing extra surface for the oxidative phosphorylation reaction (OxPhos) [2]. Trafficking of compounds between and within the different compartments is essential for function. Proteins have to be imported and processed [3,4], cytochrome *c* distributes between a soluble and a membrane bound form [5] as observed for other redox carriers, too [6]. The quality control enzyme PINK1 shuttles between cytosol, OMM and IMM [7]. During apoptosis, cytochrome *c* and other proteins are released into the cytosol [8,9], after cytosolic proteins (tBid, Drp1) are recruited to the OMM [10,11]. Owing the small diameter of mitochondria (0.5–1 μm) protein localization in different mitochondrial compartments cannot be resolved by conventional fluorescence emission microscopy. The use of fluorescence-tagged proteins is a broadly used, noninvasive way to determine protein localization. Yet, additionally to intensity based microscopy, multi-parameter fluorescence analysis can provide auxiliary information [12]. For example, the fluorescence lifetime τ of a fluorophore reports its molecular nano-environment and changes in the cellular nano-environment or at membranes can be probed [13–15]. The lifetime can be determined via its time domain after pulsed excitation and time correlated single photon counting (TCSPC) in fluorescence lifetime imaging microscopy (FLIM) [16]. The fluorescence intensity decays exponentially and the lifetime (time constant τ) is given by the time over which the fluorescence intensity drops to about 37% of its initial value. The decay in fluorescence intensity is determined by electrodynamic interactions. The transition rate (inverse lifetime) of an electric dipole emitter (fluorescing molecule) can be decomposed into a radiative and a non-radiative part as $k_{fl,0} = k_{rad} + k_{nr}$, where the index 0 indicates that this rate refers to an emitter in a homogeneous

☆ This article is part of a Special Issue entitled 'EBEC 2016: 19th European Bioenergetics Conference, Riva del Garda, Italy, July 2-6, 2016', edited by Prof. Paolo Bernardi.

* Corresponding author at: Fachbereich Biologie, Westfälische Wilhelms-Universität Münster, AG Zoologie und Molekulare Zellbiologie, Schloßplatz 5, 48149 Münster, Germany.
E-mail address: buschkar@uni-muenster.de (K.B. Busch).
URL: http://www.karin-busch.org (K.B. Busch).

http://dx.doi.org/10.1016/j.bbabio.2016.03.021
0005-2728/

medium (e.g. aqueous solution). The electrodynamic interactions range in the nanometer scale. The fluorescence decay of GFP can be correlated with the local refractive index [17], which differs between cellular compartments [18]. This is described by the Strickler–Berg formula [19], where fluorescence lifetime τ_r of fluorescent proteins is a function of the inverse refractive index n of the environment to the square (Eq. (1)):

$$\frac{1}{\tau_r} = 2.88\ x\ 10^{-9} n^2 \int \frac{I(\sigma)d\sigma}{I(\sigma)\sigma^{-3}d\sigma} \int \frac{\epsilon(\sigma)}{\sigma} d\sigma \quad (1)$$

In which n is the refractive index, I is the fluorescence emission, ε is the extinction coefficient and σ is the wavenumber.

It is conceivable that mitochondrial compartments provide different nano-environments. This is in particular valid for mitochondrial membranes with their specific composition of lipids and proteins in the OMM and IMM [5,20]. We here set out to test FLIM as a viable technique to sense and determine these specific nano-environments. In particular, we wanted to evaluate whether FLIM is a feasible method to dissect protein localization in different mitochondrial compartments, which is not possible by conventional microscopy. Our results show that FLIM indeed is a suitable method to distinguish the localization of proteins in different mitochondrial microcompartments. By determination of the fluorescence time constants of probes at different proteins we found typical differences for OMM, IMM and matrix proteins. Furthermore, FLIM was sensitive enough to record changes in the nano-environment of a specific protein.

2. Results

2.1. Characterization of mCitrine as a lifetime probe for FLIM

We used mCitrine as lifetime probe to determine the influence of the nano-environment on its fluorescence lifetime. mCitrine is an improved yellow fluorescent protein (YFP) mutant (S65G/V68L/Q69M/S72A/T203Y) with reduced sensitivity to chloride, higher resistance to acid quenching, a pK_a of 5.7, and more easily expressible at 37 °C [21]. At neutral pH, soluble mCitrine has a single fluorescent decay component [13,17]. Purified mCitrine-His_6 was dissolved in phosphate buffered saline (PBS) at 37 °C and mCitrine fluorescence decay was recorded by means of time-correlated single-photon counting (TCSPC). We determined a single exponential decay lifetime $\tau_{mCitrine} = 3.03$ ns (±0.01 ns, s.d.), which is consistent with previous reports [22]. To mimic changes in the nano-environment, increasing amounts of glycerol were added to a PBS solution. The fluorescence decay had a single component also in increasing glycerol/PBS mixtures (Figure S1). With increasing glycerol amount, we found a reduction in the lifetime of mCitrine at 37 °C as expected (Fig. 1A). The decrease followed no linear function, though. The increasing glycerol content in aqueous buffered saline (PBS) was accompanied by an increase in the refractive index (Fig. 1B) as expected [23]. When the inverse lifetime was plotted as a function of the refractive index to the square according to the Strickler–Berg-relation [19], the relation was not linear at 37 °C (Fig. 1C). The sensitivity for temperature and the moderate pH dependency in the neutral to basic range (Fig. 1D) was described before [24]. In the physiological pH range (pH 7.0–7.75) a single lifetime τ was obtained from a mono-exponential fit of the TCSPC course. The concentration of a soluble cytosolic mCitrine protein had no influence on the fluorescence lifetime (Fig. 1E). Finally, we checked for effects of reducing and oxidizing conditions on τ. While oxidizing conditions (H_2O_2 and fumigation with pure O_2) had no effect, reductive 1,4-dithiothreitol (DTT) decreased the lifetime significantly. Respiring mitochondria are oxidizing with a relative positive actual redox potential $E_{h,pH\ =\ 7}$ at the matrix site under the assumption that 10% of the NAD^+/NADH pool is reduced (resulting in $E_{h,pH\ =\ 7} = -290$ mV) and the O_2/H_2O couple contributes with $E_{h,7} = +780$ mV [25]. We thus presume oxidizing conditions for our matrix oriented probes (see below).

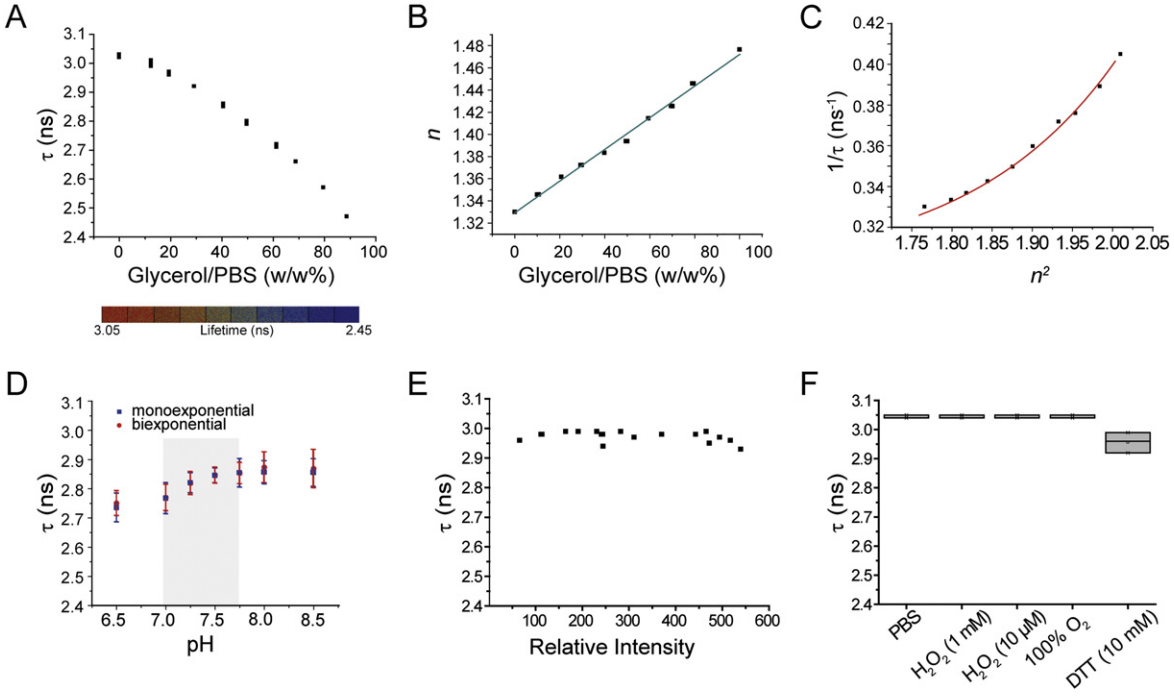

Fig. 1. mCitrine as a probe for fluorescence lifetime imaging microscopy FLIM. A) The fluorescence lifetime of mCitrine decreases with increasing amount of glycerol in aqueous glycerol/PBS mixtures (w/w%; pH 7.3) at 37 °C (triplets measured). The color scale encodes the respective lifetimes in increasing glycerol/PBS mixtures. B) The refractive index n increases with increasing glycerol/PBS mixtures (37 °C). n was determined with a heated Abbe refractometer. C) The inverse lifetime of mCitrine plotted as a function of the refractive index to the square as suggested by the Strickler–Berg relation. D) Mean lifetimes of mt-mCitrine in permeabilized cells equilibrated in incubation buffers with different pH and in presence of Oligomycin, Nigericin and CCCP. In the physiological pH range (pH 7.0–7.75), the fluorescence lifetime shows a mono-exponential decay. E) No intensity dependence was found for the lifetime of soluble mCitrine in cells. F) Influence of oxidizing and reducing conditions on the lifetime time constant τ of mCitrine.

2.2. FLIM allows for distinction of localization in different mitochondrial compartments

By conventional light microscopy it is hardly possible to locate fluorescence-labeled proteins in their mitochondrial sub-compartments. Usually, co-staining with MitoTracker dyes only reveals mitochondrial localization but not the topology in sub-compartments (Figure S2). Since mitochondrial microcompartments provide different nano-environments, we asked whether it is possible to dissect the localization of proteins in different sub-compartments of mitochondria by fluorescent lifetime imaging. First, we tested whether a probe at the OMM could be distinguished by its lifetime from a probe at the IMM and the matrix. mCitrine was fused to the C-terminus of Tom20, a receptor subunit of the translocase of the outer mitochondrial membrane (TOM), to AKAP1, an A-kinase anchor protein in the OMM, to the B-subunit of respiratory complex II (SDH), and to the 6.4 kDa subunit of *bc1* complex (complex III of the respiratory chain). Furthermore, mCitrine was targeted to the matrix by fusion to the matrix targeting (mt) sequence of the mitochondrial processing peptidase MPP (mt-FP in Fig. 2A). Mitochondrial localization was checked by fluorescence imaging of MitoTracker® stained cells expressing the respective constructs (Figure S2). The topology of the particular subunits of CII and CIII towards the matrix site was earlier shown by Immuno-EM [26]. The fluorescence intensity images of Tom20-mCitrine and *bc*1-mCitrine showed mitochondrial localization (Figure S2), but discrimination between localization in the OMM and IMM was not possible, while in the FLIM images, different lifetimes for Tom20-mCitrine and *bc*1-mCitrine are observable with a lower lifetime at *bc*1-complex at the IMM than at Tom20 at the OMM or the cytosol (Fig. 2A). The respective time constants τ were then determined by fitting the decay of the TCSPC histogram. In the plotted TCSPC diagrams of cytosolic and of *bc1*-mCitrine a clear difference is visible showing the faster decay of *bc1*-mCitrine (Fig. 2B). In addition to *bc1*-mCitrine, TSCPC diagrams were recorded and fitted for AKAP1-mCitrine, Tom20-mCitrine, CII-mCitrine and mt-mCitrine. While Tom20-mCitrine, AKAP1-mCitrine and CII-mCitrine showed no difference in τ derived from mono- or bi-exponential fits, for *bc1*-mCitrine, bi-exponential fits showed higher X^2 and smaller residuals (Figure S3). The localization in the different compartments correlated with different lifetimes: First, the lifetime of mCitrine at OMM proteins AKAP1 and Tom20 was significantly ($P \leq 0.01$) lower than of cytosolic mCitrine ($\tau = 2.92 \pm 0.03$ s.d.). AKAP1-mCitrine had a higher lifetime ($\tau = 2.88 \pm 0.02$ s.d.) than Tom20-mCitrine ($\tau = 2.87 \pm 0.01$ s.d.) (Fig. 2C). Targeting of soluble mCitrine to the matrix reduced the lifetime ($\tau = 2.84 \pm 0.03$ s.d.) significantly compared to soluble mCitrine in the cytosol ($t = 2.92 \pm 0.03$ s.d.; $P \leq 0.001$). Coupling of mCitrine to the inner membrane OxPhos complex CII was accompanied by a further reduction ($\tau = 2.81 \pm 0.03$ s.d.). The lowest lifetime was found for mCitrine at *bc1*-complex (CIII), though ($\tau = 2.77 \pm 0.02$ s.d.). Since the *bc1* complex is known to be part of OxPhos supercomplexes [27], we next checked whether the low lifetime might be dependent on macro-molecular crowding. First, we increased the amount of labeled *bc1* to enhance the probability for *bc1*-mCitrine assembly into supercomplexes. Indeed, the time constant τ decreased indicating increased interaction/molecular crowding with other proteins (Fig. 2D). Next, we stimulated respiration and biosynthesis of OxPhos complexes by substituting glucose in the medium by galactose [28]. The lifetime of mCitrine at *bc1* in galactose was significantly lower than in glucose. Last, we starved cells for 2 h in PBS, which stimulates lipid degradation in mitochondria [29]. This is supposed to imbalance protein/lipid ratio towards higher membrane protein content. Again, the lifetime was shortened under this condition indicating increased protein crowding in the IMM. Together these data suggest that the probe at the *bc1*-complex is sensitive enough to record changes in the nano-environment of a protein.

To check whether different pH affected the lifetime, we imposed identical pH conditions (pH 7.5) in the cytosol and the matrix by

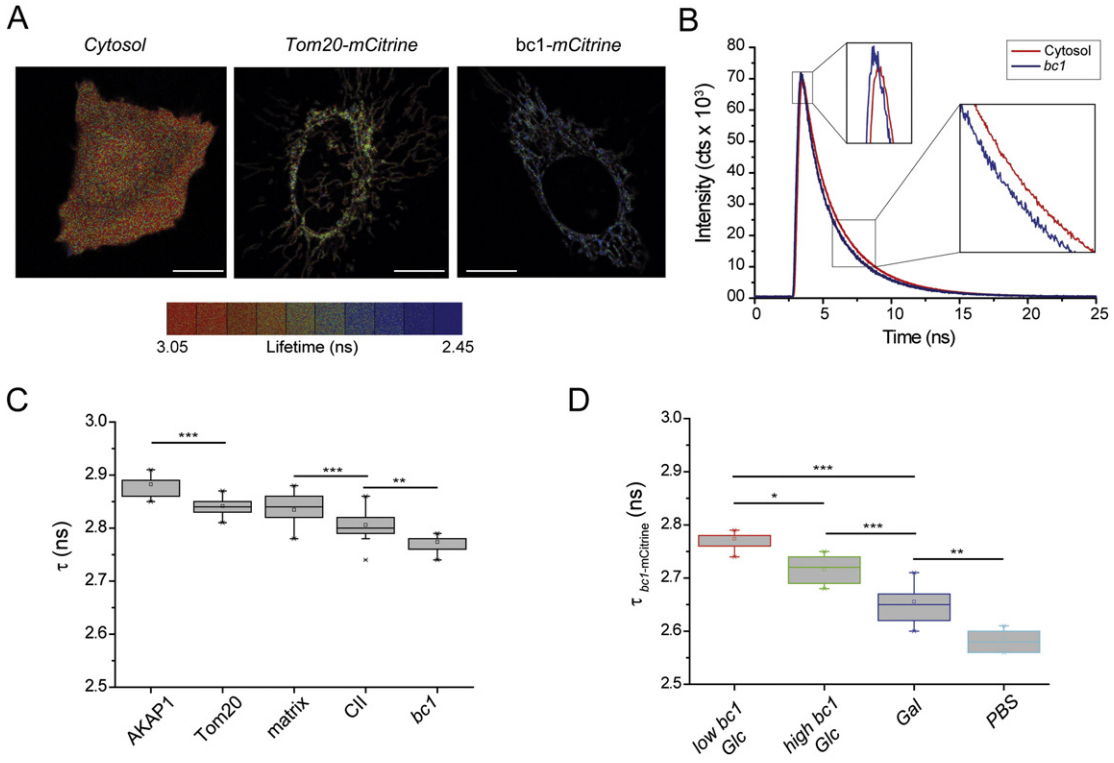

Fig. 2. Dissection of proteins in different mitochondrial microcompartments by fluorescence lifetime imaging. A) FLIM images of cells expressing mCitrine, Tom20-mCitrine and *bc1*-mCitrine. B) First excited electronic-state fluorescence decays of cytosolic mCitrine and *bc1*-mCitrine by using TCSPC. C) Time constants τ for mCitrine at the OMM (AKAP1, Tom20), the matrix and the IMM (CII, *bc1*), respectively (n = 3) with significant differences (t-test, ** $P \leq 0.01$;***$P \leq 0.001$). D) Factors influencing the nano-environment and thus lifetime of *bc1*-mCitrine: high *bc1*-mCitrine expression levels, incubation of cells in galactose and PBS (starvation of cells). Scale bars: 10 μm (A).

permeabilizing cells in the presence of CCCP/Oligomycin/Nigericin to inhibit ATP synthase and to equilibrate pH and $\Delta\Psi_m$. No significant effect was found and the differences between OMM, IMM and matrix probes were maintained (Figure S4).

2.3. Pattern-matching analysis allows the spatial dissection of proteins below resolution

The differences in lifetime raised the question, whether it is possible to discriminate between mCitrine localized in the OMM and IMM in the same cell by FLIM. To test this, we expressed mCitrine fused to AKAP1 (an OMM protein) and *bc1*-complex (IMM). By a pattern-matching algorithm [30,31] the contribution of AKAP1-mCitrine photons and *bc1*-mCitrine photons to each pixel was calculated (Fig. 3A). Photons of each pixel were assigned to either of the pattern (X(i) = AKAP1 and Y(i) = *bc1*-mCitrine, with X(i) + Y(i) = P(i) as total number of photons in the pixel). The X(i) and Y(i) were scaled to numbers between 0 and 255 according to r(i) = floor(255 ∗ X(i) / M) and g(i) = floor(255 ∗ Y(i) / M) (M: Maximum of all X(i) and Y(i) values in the image; M = max(max(X(i), max(Y(i))). The RGB colored image was then built using the r(i) numbers for the red channel (contribution of AKAP1-mCitrine) and the g(i) numbers for the green channel (contribution of *bc1*-mCitrine).

The fluorescence decay of mCitrine in co-expressing cells showed a course in between the decays of *bc1*-mCitrine (Fig. 3B) and AKAP1-mCitrine in cells expressing only one of the protein constructs. The resulting time constant τ resulting from a bi-exponential fit of the TCSPC diagram was clearly a mixture of AKAP1-mCitrine and *bc1*-mCitrine fluorescence lifetime (Fig. 3C). When two OMM proteins AKAP1-mCitrine and Tom20-mCitrine were co-expressed, the resulting average time constant τ also showed a trend to be a mixed τ between the lifetimes for the single mCitrine constructs (Fig. 3D). These results clearly show that the distinction of localization in different mitochondrial sub-compartments is possible with FLIM, even below resolution.

2.4. The morphology of mitochondria does not mitigate the lifetime of a probe

We next asked, whether mitochondrial morphology influences the lifetime of a mitochondrial FLIM probe. We compared τ values of mt-mCitrine in tubular and fragmented mitochondria in cells incubated in medium with different pH. Mitochondria were classified as fragmented, when the length/width ratio was smaller than 3. In cells with normal matrix pH (pH 7.5–8.5), no difference in the mean lifetime of the matrix probe was found between tubular and fragmented mitochondria, but in the fragmented mitochondria, the overall variation (standard deviation σ) was higher (Fig. 4A). This was observed for all tested pH (pH 6.5, pH 7.0 and pH 7.25): increased heterogeneity of the sample, but no change in the respective mean lifetimes. The heterogeneity of fragmented mitochondria is shown in Fig. 4B. Next, we compared τ values of CII-mCitrine and *bc1*-mCitrine in normal cells and cells with increased mitochondrial fragmentation caused by hFis1 overexpression. hFis1 is known as a mitochondrial fission factor [32]. Also in fragmented mitochondria resulting from hFis overexpression, no change in τ was observed for CII-mCitrine or *bc1*-mCitrine (Fig. 3C, D). Thus, mitochondrial morphology does not mitigate the fluorescence lifetime of a probe in the mitochondrial matrix or at the IMM.

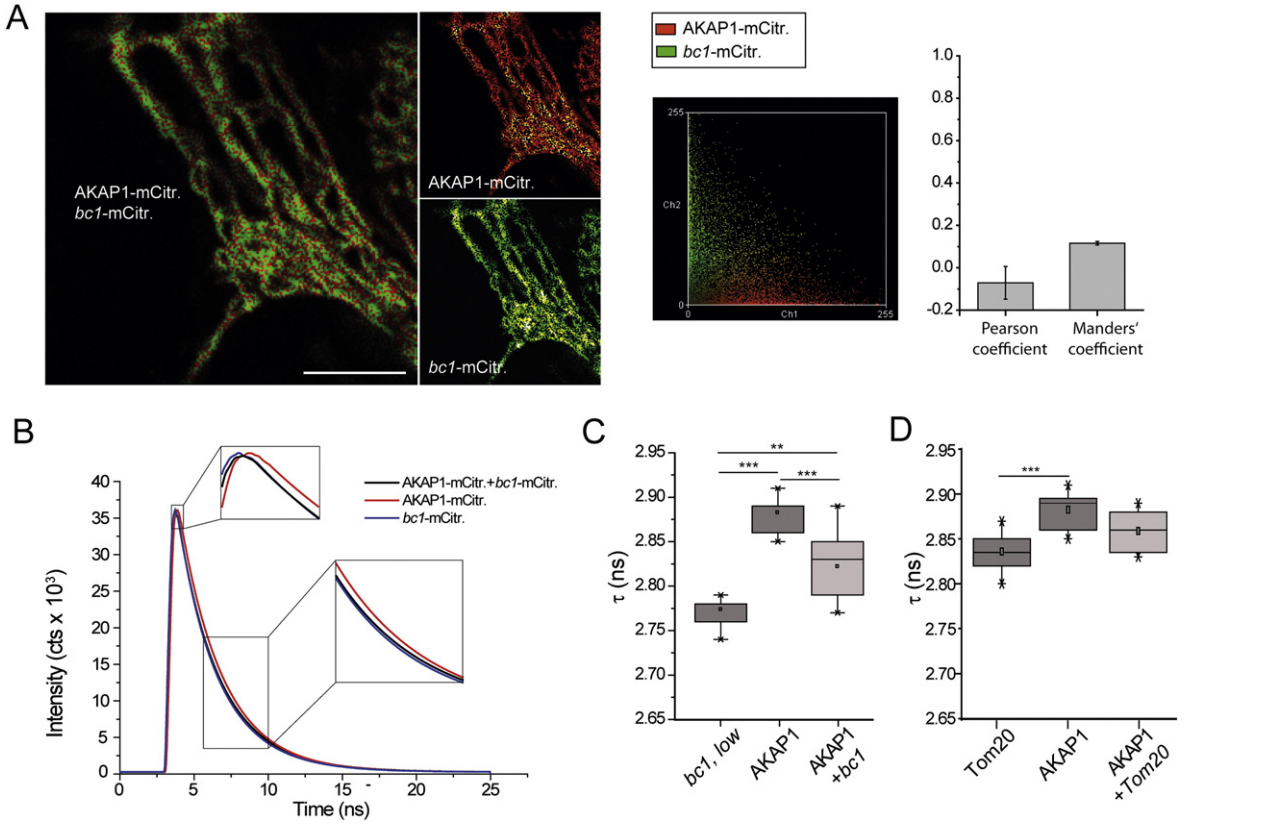

Fig. 3. Sub-diffraction analysis of protein localization in different mitochondrial microcompartments by lifetime imaging. A) Pattern based analysis of the original FLIM image of cells co-expressing AKAP1-mCitrine and *bc1*-mCitrine. The red channel shows the AKAP1-mCitrine contribution, the green channel the *bc1*-mCitrine contribution. The inset in the composite shows the co-localization analysis using the ImageJ® plugin for colocalization analysis to determine the Pearson and Manders' coefficients. B) Normalized TCSPC diagrams of AKAP1-mCitrine (red) and *bc1*-mCitrine (blue) fluorescence from single transfected cells and from a double-transfected cell line (AKAP-mCitrine + *bc1*-mCitrine, black). C) Mean τ values for double and single transfection: AKAP1-mCitrine + *bc*1-mCitrine and AKAP1-mCitrine and Tom20-mCitrine, respectively. Scale bars: 10 μm (A).

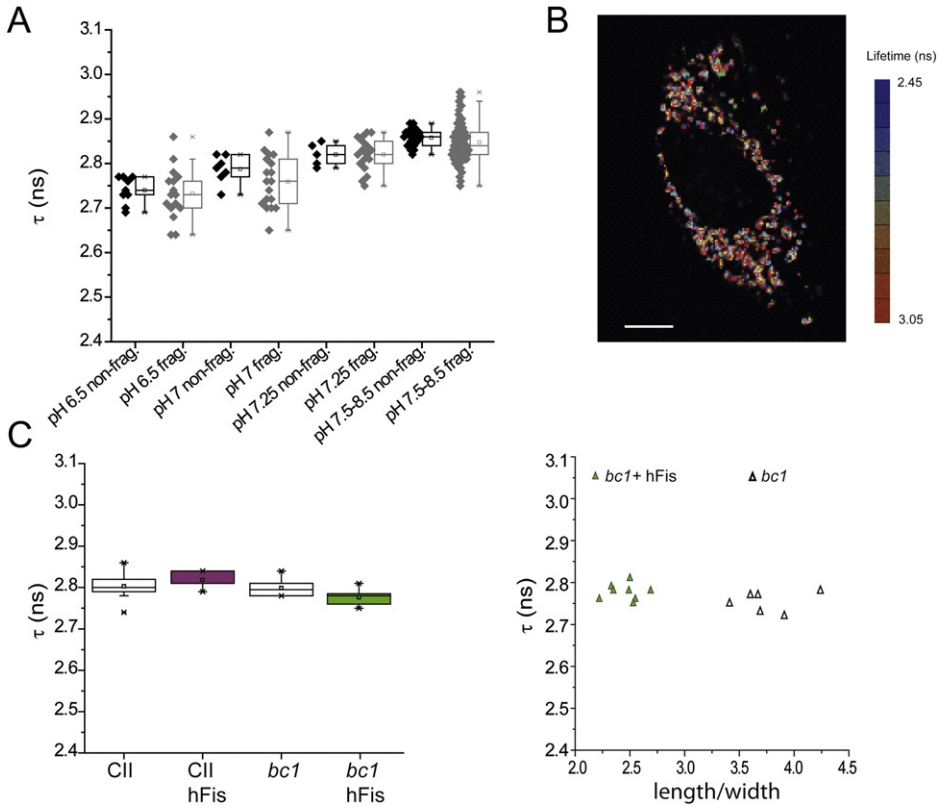

Fig. 4. The morphology of mitochondria has no influence on the mean τ value. A) Box and Whiskers plot showing the lifetime of mt-mCitrine in tubular (length:width ≥ 3) and fragmented (length:width < 3) mitochondria at different pH values. Mitochondrial pH ranges usually between pH 7.5–8.0. Equilibration at different pH was achieved by incubation of permeabilized cells in different buffers (pH 6.5, pH 7.0 and pH 7.25) with CCCP/Oligomycin/Nigericin to uncouple respiration and to inhibit ATP synthesis. Fragmentation increases σ (standard deviation), but the mean time constant τ was unaffected. B) Lifetime image showing the heterogeneity of fragmented mitochondria. Scale bar: 10 μm. C) Left site: lifetimes of CII-mCitrine or *bc1*-mCitrine in normal cells and cells overexpressing hFis. Right site: Plot showing the lifetimes in relation to the aspect ratio (length/width) of mitochondria.

2.5. Shifts of PINK1 localization in polarized and depolarized mitochondria are monitored by FLIM

The phosphatase and tensin homologue Pten-induced kinase 1 (PINK1), one sensor for mitochondrial integrity, is a cytosolic protein that is processed in mitochondria with an intact membrane potential. During its processing, full-length PINK1 is completely imported into mitochondria, proteolytically processed and a short form is released to the cytosol again. Superresolution imaging recently revealed that PINK1 co-localized with the IMM-protein Complex I (NADH:ubiquinol:oxidoreductase) [7]. Obliteration of the mitochondrial membrane potential by CCCP prevented the import and resulted in an accumulation of PINK1 at the mitochondrial surface [7,33]. We asked, whether FLIM would be able to monitor this shift in PINK1 location under the respective circumstances. Intensity images of PINK1-mCitrine showed cytosolic PINK1-mCitrine when the expression level was high and predominantly mitochondrial localization at moderate expression levels (Figure S6 A) related to high turnover rates and low steady state levels of PINK1 [34]. The averaged time constant τ from the entire cell was in between mitochondrial ($\tau = 2.91 \pm 0.03$ ns; s.d.) and cytosolic mCitrine ($\tau = 2.99 \pm 0.02$ ns; s.d.) (Fig. 5A). Next, we determined the lifetime in depolarized mitochondria. Comparison of the lifetime in single cells before and after CCCP addition showed an increase of the lifetime after CCCP treatment in 8 out of 10 cells. Since we can exclude a morphological effect (mitochondria fragment after CCCP addition) (Section 2.4), this apparently results from the retention of PINK1-mCitrine at the mitochondrial surface in depolarized mitochondria. The lifetime in depolarized mitochondria was in between the lifetime of the probe in untreated cells that had only low (mitochondrial) levels of PINK1 and that with high (cytosolic) levels of PINK1-mCitrine (Fig. 5C, E), indicating a shift towards cytosolic localization. Finally, we recorded the lifetime of PINK-95A-mCitrine. This mutant was reported to have an attenuated processing [35]. After CCCP application, the trend was towards higher τ values (Fig. 5D). Again, this can be interpreted as an increased quota of PINK1-P95A-mCitrine remaining in the cytosol. Together, our lifetime data are in line with the model of PINK1-shuttling through actively respiring mitochondria and retention outside depolarized mitochondria [7,36].

2.6. Protein translocation to membranes is accompanied by a reduction in fluorescence lifetime

Lifetime imaging of PINK1-mCitrine was sensitive enough to distinguish different proteins located in different mitochondrial subcompartments and also to monitor shifts in the location of a single protein. This led us to ask whether also protein translocation within a single compartment could be monitored by FLIM. In order to test this, we induced translocation of cytosolic mCitrine to the OMM and of matrix mCitrine to the IMM. This was achieved by chemically initiated complex formation between FRB-mCitrine and a FKBP-membrane protein by addition of rapamycin. Rapamycin is an organic molecule working as a chemical inducer of dimerization (CID). The resulting in ternary complex formation FRB:rapamycin:FKBP is rather stable ($K_d = 12 \pm 0.8$ nM [37]). The outer (Tom20) and inner membrane (*bc*1) proteins were fused to the FK506 binding protein FKBP12 and the mCitrine-probe was linked to the FKBP-rapamycin-binding (FRB) domain of mTOR (mechanistic target of rapamycin) (Fig. 6A). Ternary complex formation of FRB-mCitrine:rapamycin:FKBP *per se* had no influence on $\tau_{mCitrine}$, as tested with FRB-mCitrine and FKBP (Fig. 6B). Since FKBP-anchor proteins were not fluorescent in the assays, FKBP-membrane

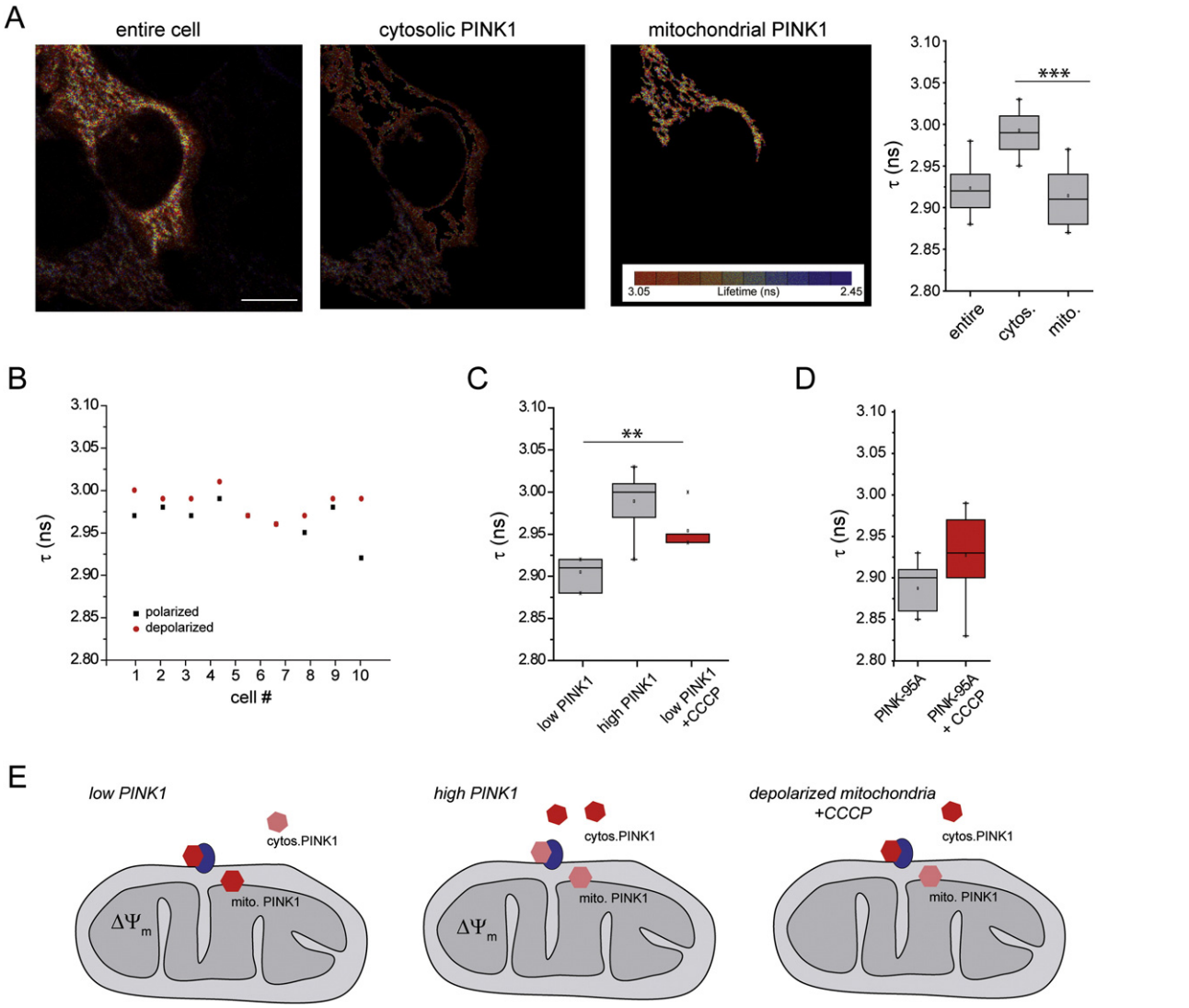

Fig. 5. FLIM monitors shifts in cytosolic and mitochondrial PINK1 distribution. A) FLIM images of a cell with cytosolic and mitochondrial PINK1-mCitrine that possess significantly different lifetime τ. B) Mean lifetime of PINK1-mCitrine in single cells before and after chemical depolarization of mitochondria by CCCP (1 μM) addition. C) Time constants τ for PINK1-mCitrine in cells with low expression level, in cells with high expression level and in cells with depolarized mitochondria (n = 3). D) Time constants τ for PINK1-95A-mCitrine in cells before and after CCCP treatment. E) Schemes showing the distribution of PINK1-mCitrine under the different conditions tested (red hexagon: PINK1-mCitrine; light red hexagon: reduced levels of PINK1-mCitrine; blue: Tom20) according to [7]. Scale bar: 10 μm (A).

proteins were also expressed as GFP fusion proteins in a parallel assay to verify their correct localization. For the matrix translocation assay, a bicistronic IRES-vector were constructed with the FKBP-membrane protein at first place and the soluble mt-FRB-mCitrine at second to ensure the co-expression of the fluorescent and non-fluorescent proteins. Before the addition of rapamycin, FRB-mCitrine was homogenously distributed in the cytosol as the FLIM image shows (Figs. 2A, 6C). Then, we initiated ternary complex formation of soluble FRB-mCitrine with Tom20-FKBP by rapamycin addition. Within 2 min after induction, mitochondria-localized signals appeared (supplementary video 1). From TCSPC histograms, the fluorescence lifetimes were determined. The resulting lifetimes for FRB-mCitrine before and 20 min after rapamycin addition were significantly different with a lower lifetime of FRB-mCitrine at the Tom20-FKBP complex. Still, the lifetime was higher than that of mCitrine directly attached to Tom20 (Fig. 6C). The same assay was repeated with Tom20-Halo7-FKBP and soluble FRB-sEcGFP, a GFP derivative [38], to exclude an artifact caused by the fluorescent protein. Tom20-Halo7-FKBP was visualized by addition of TMR-^{HTL} substrate [7] (Figure S7). Single cells were monitored for 70 min after rapamycin addition. The lifetime of sEcGFP decreased continuously due to translocation of the soluble FRB-sEcGFP to the membrane caused by rapamycin-induced ternary complex formation between FRB-sEcGFP and Tom20-Halo7/TMR^{HTL}-FKBP (Figure S7 B). 60 min after rapamycin addition, most of the FRB-sEcGFP was at the OMM and no further change was observed anymore. Since the stoichiometric ratio between a soluble and a membrane-protein is not expected to be equal, part of the FRB-sEcGFP remained unbound in the cytosol resulting in a background signal. The assay was also performed with mt-mCitrine-FRB and *bc1*-FKBP. After rapamycin addition, no changes were visible in the intensity image, but the FLIM image reported a significant decrease in lifetime (Fig. 7D). TCSPC fluorescence decays were fitted with a bi-exponential fit (Figure S5). We attribute this to successful complex formation at the *bc1*-complex in the IMM.

3. Discussion

Sub-compartmental localization of proteins is often difficult to resolve by conventional light microscopy due to the Abbe limit of diffraction. Even more challenging is to dissect the translocation of proteins between or within cellular compartments such as mitochondria. Here,

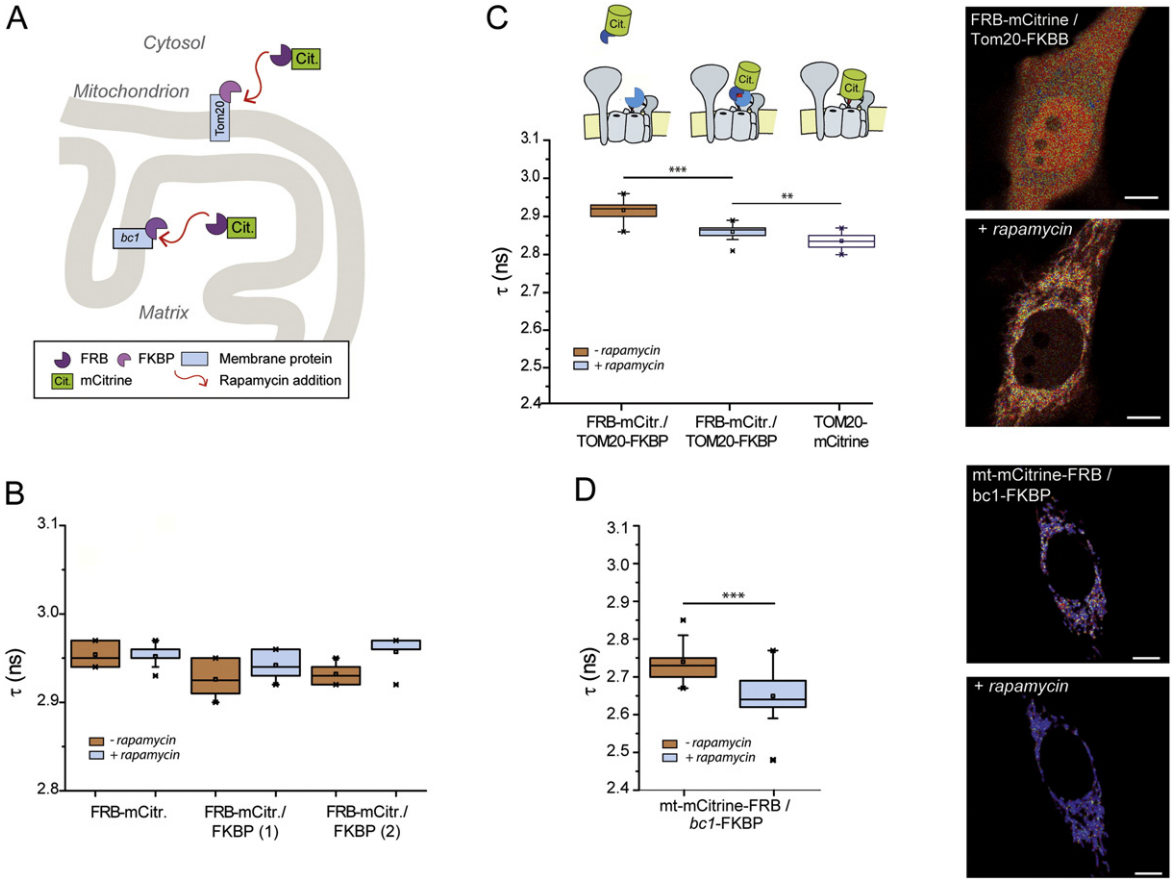

Fig. 6. FLIM records protein complex formation of mCitrine with proteins at the outer and inner mitochondrial membrane. A) Scheme of experimental set-up to induce translocation of FRB-mCitrine from the cytosol to Tom20-FKBP at the OMM and mt-mCitrine to *bc1*-FKBP at the IMM by ternary complex formation. B) Complex formation between soluble FRB-mCitrine and FKBP had no effect on $\tau_{mCitrine}$. Two independent experiments are shown. C) Changes of fluorescence lifetime due to the translocation of mCitrine from the cytosol to Tom20 at the OMM in comparison to lifetime τ of Tom20-mCitrine. D) Induced transfer of mt-mCitrine from the matrix to the IMM-protein *bc1*-complex at the matrix site. FLIM of single cells was performed before and 20 min after rapamycin addition and the fluorescence lifetime was determined from the TCSPC histograms. Mean τ derived from n = 3 independent experiments (s.d.), statistics: Students t-Test (***: $P < 0.001$; **:$P \leq 0.01$).

we addressed this problem by fluorescence lifetime imaging microscopy (FLIM). We demonstrate that lifetime variations are determined by the respective protein nano-environment in mitochondrial compartments. FLIM in combination with FRET is best known as a method to prove protein–protein interactions, but it is also a technique to sense the nano-environment of proteins [39,40], which changes due to activation processes. So it was shown, that the lifetime of a GFP-tagged major histocompatibility complex class I protein was shortened at the inhibitory NK cell IS at an immunological synapse [14]. We compared soluble mCitrine with Tom20- and AKAP1-mCitrine at the OMM and with CII- and *bc1*-mCitrine at the IMM and found that the membrane protein-mCitrines had a shortened lifetime compared to the soluble form. This is in agreement with what was observed before for soluble GFP and GFP at surfaces [14]. To check, whether the membrane *per se* influences the lifetime, we modeled the effect of an interface close to the emitter. However, the data suggest, the influence of a membrane *per se* on the fluorescence lifetime of a probe is negligible (Figure S8). Therefore other factors might cause the attenuation of the lifetime of membrane proteins. In general, mitochondrial membranes are very protein-rich (up to 65% w/w lipids) [5,41]. Tom20 at the outer mitochondrial membrane is part of the TOM machinery and probably co-localizes with import proteins, chaperones and likely also ribosomes. This protein nano-environment provides manifold possibilities for electrodynamic interactions to enhance the transition rate $k_{fl,0}$ and thus decrease the lifetime. mCitrine at AKAP1 also had a reduced lifetime compared to cytosolic mCitrine, but to a smaller extend. Owing its numerous interaction partners [42], AKAP1 can be seen as a multicomponent system, too. In both cases (Tom20 and AKAP1) molecular crowding and thus enhanced possibility of electro-dynamic interactions might well account for the observed reduced lifetimes of the probe. The lifetimes of probes at inner mitochondrial membrane complex CII and *bc1*-complex (CIII) were further reduced. Coincidently, the IMM has an even higher quota of proteins than the OMM, several of them forming macromolecular protein complexes [43]. Strikingly, mCitrine at CII, which is in contrast to the *bc1*-complex not part of a supercomplex [44,45], had a significantly higher lifetime than *bc1*-mCitrine. Furthermore, *bc1*-mCitrine was sensitive for changes in the IMM architecture and composition induced by stimulation of respiration or by starvation. In both cases, the re-organization of the IMM is probably accompanied by an increase in protein/lipid ratio: galactose induces the synthesis of OxPhos proteins [28], while starvation stimulates β-oxidation of lipids [29]. We have indications (in preparation) that starvation also induced lipid degradation from the IMM, thereby enhancing the protein/lipid ratio. An increased protein/lipid ratio would result in higher crowding for proteins in the IMM, reflected by a lifetime decrease.

Next, we investigated whether it is possible to distinguish between mCitrine localized at the OMM, IMM and in the matrix in the same cell by recording fluorescence lifetimes. Recent work demonstrated the power of FLIM for efficient identification of fluorophore ratios in complex multidimensional fluorescence signals using reference fluorescence decay by pattern-matching technique [46]. We co-expressed mCitrine fused to an OMM-located protein (AKAP1) and mCitrine

fused to the *bc1*-complex in the IMM. By patterned analysis of mCitrine lifetime and location, we dissected the lifetimes of mCitrine corresponding to OMM and IMM location in every pixel and found hardly co-localization of the corresponding channel pixels. The averaged time-constant from the bi-exponential fit was in between the time constants of the singular proteins. Also, in cells co-expressing Tom20- and AKAP1-mCitrine, the averaged lifetime was in between the lifetimes for singular proteins. These results show that it is in principle possible to discriminate the localization of proteins labeled with the same fusion-protein in the OMM and IMM and with further optimization (spectral unmixing [46], mCitrine and GFP) eventually also for the same mitochondrial compartment.

The different lifetimes in aqueous environments and at cellular membranes allowed then for recording translocation of soluble proteins to a membrane-site. By rapamycin-induced formation of a ternary complex between FRB-mCitrine, rapamycin and a membrane-anchored FKBP, we monitored the FRB-mCitrine translocation to Tom20 at the OMM (which is also detectable in fluorescence images), and to *bc1*-complex from the matrix site (which is not visible in fluorescence intensity images). However, the sensitivity of FLIM was sufficiently high to monitor this translocation inside mitochondria.

Several tasks in active mitochondria are linked to protein translocation. One example is the maturation of PINK1, associated with diverse quality control mechanisms [47], inside mitochondria. During this process, PINK1 is disseminated at least between three compartments (cytosol, OMM, and IMM) as we recently showed by triple color superresolution microscopy [7]. To test, whether lifetime variations would indicate the re-distribution of PINK1, we performed FLIM with PINK1-mCitrine and PINK1-95A-mCitrine, a mutant with retarded maturation inside mitochondria [35] in normal and de-energized mitochondria. Under low expression conditions, PINK1-mCitrine was predominantly found in mitochondria with a time constant higher than for AKAP1-mCitrine and Tom20-mCitrine. We attribute this to the fast shuttling of soluble PINK1 through mitochondria and only transient interaction with other proteins. In depolarized mitochondria, the lifetime increased for PINK1-mCitrine and PINK1-95A-mCitrine in line with retention at the mitochondrial surface [33]. Thus, variations in the lifetime reflected changes in the localization in accordance with biochemical and superresolution data. In principle all variations in lifetime are related to distinct nano-environments. To describe the nano-environment, the refractive index *n* was used beforehand [17,39]. At room temperature, the fluorescence lifetime is as a linear function of the inverse refractive index *n* to the square [19,23]. However, this relation valid for room temperature was no longer appropriate at 37 °C. Thus, a direct translation of mCitrine lifetimes into local refractive indices is difficult and would require thorough calibration. In this context, it would be helpful to relate FLIM data with optical properties gained from holographic interferometric detection microscopy to assess local refractive indices accurately by phase imaging [48].

In summary, we have demonstrated that FLIM is a powerful technique that allows for probing distinct protein localization and translocation between and within mitochondrial compartments. Explicitly, its sensitivity in the time domain (TCSPC) allows for surpassing the limits set by diffraction. This is especially promising to monitor protein dynamics inside organelles beyond resolution.

4. Conclusions

The fluorescent lifetime of a probe is dependent on its immediate environment, which is specific for each sub-compartment of the cell including mitochondria. We here demonstrate that fluorescence lifetime imaging microscopy (FLIM) can be used to probe protein localization and dynamics inside mitochondria that are usually not accessible by conventional imaging. Our data suggest that macromolecular crowding is the predominant factor determining the lifetime of a specific probe. Especially for studying organelles fluorescence lifetime recording is an auxiliary tool to address events below the diffraction limit in live cells.

5. Materials and methods

5.1. Cloning of sensor proteins

FRB-mCitrine was assembled behind the IMMV promoter in the pSems26-Vector from @NEB, substituting the original snap-ORF. For measurements in the cytosol, this vector was used for expression. For measurements in the matrix, the N-terminal 60 amino acid residues indicated as the mitochondrial targeting sequence of MPP (MPP60) were included at the 3′end of mCitrine-FRB resulting in mt-mCitrine-FRB. This mt-sequence is likely removed in the mitochondrial matrix by the mitochondrial processing peptidase MPP. For chemically induced translocation via FRB:rapamycin:FKBP complex formation in the matrix, an IRES vector was created with the anchor proteins *bc1*-FKBP behind the IMMV-promotor followed by the FRB-mCitrine. Tom-mCitrine was constructed with a linker of 3 amino acid residues between the Tom20-terminus and mCitrine N-terminus. One additional amino acid residue was placed between AKAP1 and mCitrine. PINK1-mCitrine and PINK1-P95A-mCitrine were generated by substituting the HaloTag from constructs recently described [7]. All open reading frames for cloning were obtained from a self-made cDNA bank from HeLa cells, and plasmids were sequenced before use.

5.2. Fluorescent lifetime τ in increasing glycerol solutions

The aqueous glycerol mixtures (0, 10, 20, 30, 40, 50, 60, 70, 80 and 90% w/w) were prepared by mixing glycerol (Roth: spectrophotometric grade, ≥99.5%) with phosphate buffered saline (PBS) pH 7–7.5 (PAA Biotech). The purified protein His6-mCitrine was diluted to a final concentration of 4.6 μM. The samples were prepared and lifetime was measured at 37 °C in 500 μL multiwell plates (Ibidi®) in triplets. In parallel, the refractive index of the same solutions was determined with an Abbe-refractometer heated to 37 °C.

5.3. Determination of the pH dependence of fluorescent lifetime τ

The pH dependence of the mCitrine lifetime was performed with living cells expressing mt-mCitrine in the matrix of mitochondria. For measurements, cells expressing mt-mCitrine were permeabilized and incubated in buffers with different pH [35]. To exclude any interference with mitochondrial activity, oxidative phosphorylation was uncoupled and inhibited by treatment with CCCP (10 μM), Nigericin (1 μM) and Oligomycin (5 μg/ml). pH dependence of the lifetime was independently measured twice in permeabilized cells.

5.4. Fluorescent lifetime τ under oxidizing and reducing conditions

For probing the influence of oxidizing and reducing conditions on the lifetime constant τ of mCitrine, aqueous solutions of His6-mCitrine in PBS with a final concentration of 4.6 μM were prepared as described before (5.2). For probing oxidizing conditions His6-mCitrine was treated with H_2O_2 (Rotipuran® p.a., ISO, stabilised, Roth) with a final concentration of 1 mM, respectively 10 μM and incubated for 15 min. In a further experimental approach the His6-mCitrine/PBS-solution was fumigated with pure oxygen for 3 min and the lifetime was determined afterwards. To identify the influence of reducing conditions His6-mCitrine was incubated with DL-Dithiothreitol (Sigma Aldrich) with a final concentration of 10 mM for 15 min.

5.5. Cell culture and transfection technique

HeLa cells were grown in culture flasks as monolayers in Minimal Essential Medium (MEM) with Earles salts containing 5.6 mM glucose,

2 mM stable glutamine and sodium bicarbonate, supplemented with 10% (v/v) fetal bovine serum (FBS), 1% nonessential amino acids (NEAA) and 1% 2-(4-(2-Hydroxyethyl)-1-piperazinyl)-ethansulfonsäure (HEPES). The cells were incubated under human physiological conditions at 37 °C with 5% CO_2 and 100% humidity. To stimulate respiration, the glucose medium was replaced with galactose medium (Dulbecco's MEM (PAA, E15–079)) with NEAA, without glucose, and supplemented with 10 mM galactose (Sigma), 4 mM glutamine (Biochrom), 10% (v/v) fetal bovine serum (FBS) superior (Biochrom), sodium bicarbonate (PAA) and HEPES (PAA) for at least 2 days. To starve cells, incubation medium was substituted by PBS containing Mg^{2+}/Ca^{2+} salts for 2 h.

For microscopy studies, $1x10^5$ cells were seeded on a glass-coverslip in a 3.5 cm cell culture dish and transiently transfected by calcium phosphate precipitation as described earlier [49]. To achieve low respectively high cellular expression levels of *bc1*-mCitrine, the transient transfection via calcium phosphate precipitation was performed with different contents of plasmid DNA (2.5 μg DNA for low *bc1*-mCitrine and 5 μg DNA for high *bc1*). About 18 h after transfection, the cells were washed twice with PBS and fresh growth medium was added. Live cell imaging was performed 48 h after transfection.

5.6. Fluorescence microscopy

The fluorescence intensity imaging and co-localization studies were performed using a confocal laser scanning microscope (Fluo-View FV1000, Olympus) equipped with a continuous 488 nm laser. A 60× oil-immersion objective (UPLSAPO oil, NA 1.35, N/0.17/FN26.5, Olympus), which was upgraded with an objective heater (BIOPTECHS), was used. Image analysis and image processing were performed using ImageJ (National Institutes of Health). For proof of mitochondrial localization of constructs, mitochondria were stained with 100 nM Mito-Tracker-DeepRed FM.

5.7. FLIM-TCSPC

Time-resolved fluorescence measurements were performed using a confocal laser scanning microscope (FluoView FV1000, Olympus) equipped with a TCSPC extension module (PicoQuant GmbH). The excitation source was a pulsed LDH-D-C-485 laser (PicoQuant GmbH) operated at a repetition time rate of 40 MHz. The output pulses were coupled into an optical fiber. The output at the fiber end was reflected from a beam splitter onto the base of a multiwell plate (Ibidi®, 30 μL) or a glass cover slip via a 60× oil-immersion objective (UPLSAPO oil, NA 1.35, N/0.17/FN26.5, Olympus) upgraded with an objective heater (BIOPTECHS). For photon detection a single photon avalanche diode (SPAD) was used. The acquisition was performed until at least 1000 photons in the brightest pixel were reached. To obtain the fluorescence lifetime of mCitrine, data analysis was performed with SymphoTime software (64 bit) and a mono-exponential tail fit with χ^2 minimization. The resulting values for the fluorescence lifetime were displayed on a standard false-color scale. The dwell time was 2 μs per pixel.

5.8. Fluorescent lifetime τ measurements in depolarised mitochondria

HeLa cells were grown in culture flasks as monolayers in Minimal Essential Medium (MEM) with Earles salts and incubated as described in 5.4. For microscopy studies, 1×10^5 cells were seeded on a glass-coverslip in a 3.5 cm cell culture dish. For low PINK1-mCitrine and PINK-95A-mCitrine the cells were transiently transfected by calcium phosphate precipitation as described earlier [49]. To achieve high expression levels of PINK1-mCitrine, the transient transfection was performed with Effectene™ Transfection Reagent (QIAGEN). About 8 h after transfection, the cells were washed twice with PBS and fresh growth medium was added. Live cell imaging was performed 24 h after transfection. For chemical depolarization, HeLa cells were treated with CCCP to a final concentration of 1 μM and incubated for 30 min before measurements. Depolarization of mitochondria under these conditions was shown before [7].

5.9. Data analysis

Fluorescence lifetime changes were measured for entire cells respectively the mitochondrial area determined by a mask. After rapamycin application, the mean lifetime of regions of interest (rois) from single cells was determined every 5–10 min. All *P* values are from 2-tailed t-tests until otherwise listed. The null hypothesis for all tests stated that the mean was equal to zero.

Supplementary data to this article can be found online at http://dx.doi.org/10.1016/j.bbabio.2016.03.021.

Transparency document

The Transparency document associated with this article can be found, in online version.

Acknowledgements

We thank Giulia Nebel and Michael Timme for important preliminary studies on the subject. This work was supported by the German National Research Foundation grant Bu2288 and the SFB944.

Author's contributions: AC-S and B-R performed and analyzed experiments and interpreted data, W-K provided important technical assistance, I-G analyzed experiments, J-E performed computational analysis, KB-B conceived the project, analyzed and interpreted data, and wrote the manuscript.

References

[1] C.A. Mannella, The relevance of mitochondrial membrane topology to mitochondrial function, Biochim. Biophys. Acta 1762 (2006) 140–147.
[2] R.W. Gilkerson, J.M. Selker, R.A. Capaldi, The cristal membrane of mitochondria is the principal site of oxidative phosphorylation, FEBS Lett. 546 (2003) 355–358.
[3] D. Mokranjac, W. Neupert, Thirty years of protein translocation into mitochondria: unexpectedly complex and still puzzling, Biochim. Biophys. Acta 1793 (2009) 33–41.
[4] A. Chacinska, C.M. Koehler, D. Milenkovic, T. Lithgow, N. Pfanner, Importing mitochondrial proteins: machineries and mechanisms, Cell 138 (2009) 628–644.
[5] M. Hochli, C.R. Hackenbrock, Lateral translational diffusion of cytochrome c oxidase in the mitochondrial energy-transducing membrane, Proc. Natl. Acad. Sci. U. S. A. 76 (1979) 1236–1240.
[6] C.G. Bowsher, L.M. Eyres, J.O. Gummadova, P. Hothi, K.J. McLean, A.W. Munro, N.S. Scrutton, G.T. Hanke, Y. Sakakibara, T. Hase, Identification of N-terminal regions of wheat leaf ferredoxin NADP + oxidoreductase important for interactions with ferredoxin, Biochemistry 50 (2011) 1778–1787.
[7] F.R. Beinlich, C. Drees, J. Piehler, K.B. Busch, Shuttling of PINK1 between mitochondrial microcompartments resolved by triple-color superresolution microscopy, ACS Chemical Biology, 2015.
[8] J. Parrish, L. Li, K. Klotz, D. Ledwich, X. Wang, D. Xue, Mitochondrial endonuclease G is important for apoptosis in *C. elegans*, Nature 412 (2001) 90–94.
[9] G. Kroemer, L. Galluzzi, C. Brenner, Mitochondrial membrane permeabilization in cell death, Physiol. Rev. 87 (2007) 99–163.
[10] Y. Zaltsman, L. Shachnai, N. Yivgi-Ohana, M. Schwarz, M. Maryanovich, R.H. Houtkooper, F.M. Vaz, F. De Leonardis, G. Fiermonte, F. Palmieri, B. Gillissen, P.T. Daniel, E. Jimenez, S. Walsh, C.M. Koehler, S.S. Roy, L. Walter, G. Hajnoczky, A. Gross, MTCH2/MIMP is a major facilitator of tBID recruitment to mitochondria, Nat. Cell Biol. 12 (2010) 553–562.
[11] D.-F. Suen, K.L. Norris, R.J. Youle, Mitochondrial dynamics and apoptosis, Genes Dev. 22 (2008) 1577–1590.
[12] S. Weidtkamp-Peters, S. Felekyan, A. Bleckmann, R. Simon, W. Becker, R. Kuhnemuth, C.A. Seidel, Multiparameter fluorescence image spectroscopy to study molecular interactions, Photochem. Photobiol. Sci. 8 (2009) 470–480.
[13] A.A. Heikal, S.T. Hess, G.S. Baird, R.Y. Tsien, W.W. Webb, Molecular spectroscopy and dynamics of intrinsically fluorescent proteins: coral red (dsRed) and yellow (Citrine), Proc. Natl. Acad. Sci. U. S. A. 97 (2000) 11996–12001.
[14] B. Treanor, P.M. Lanigan, K. Suhling, T. Schreiber, I. Munro, M.A. Neil, D. Phillips, D.M. Davis, P.M. French, Imaging fluorescence lifetime heterogeneity applied to GFP-tagged MHC protein at an immunological synapse, J. Microsc. 217 (2005) 36–43.
[15] T. Ito, S. Oshita, T. Nakabayashi, F. Sun, M. Kinjo, N. Ohta, Fluorescence lifetime images of green fluorescent protein in HeLa cells during TNF-alpha induced apoptosis, Photochem. Photobiol. Sci. 8 (2009) 763–767.

[16] P.I. Bastiaens, A. Squire, Fluorescence lifetime imaging microscopy: spatial resolution of biochemical processes in the cell, Trends Cell Biol. 9 (1999) 48–52.
[17] K. Suhling, J. Siegel, D. Phillips, P.M. French, S. Leveque-Fort, S.E. Webb, D.M. Davis, Imaging the environment of green fluorescent protein, Biophys. J. 83 (2002) 3589–3595.
[18] J. Beuthan, O. Minet, J. Helfmann, M. Herrig, G. Muller, The spatial variation of the refractive index in biological cells, Phys. Med. Biol. 41 (1996) 369–382.
[19] S.J. Strickler, R.A. Berg, Relationship between absorption intensity and fluorescence lifetime of molecules, J. Chem. Phys. 37 (1962) (814-&).
[20] R.R. Chance, A. Prock, R. Silbey, Lifetime of an emitting molecule near a partially reflecting surface, J. Chem. Phys. 60 (1974) 2744–2748.
[21] O. Griesbeck, G.S. Baird, R.E. Campbell, D.A. Zacharias, R.Y. Tsien, Reducing the environmental sensitivity of yellow fluorescent protein. Mechanism and applications, J. Biol. Chem. 276 (2001) 29188–29194.
[22] B. Sands, P. Jenkins, W.J. Peria, M. Naivar, J.P. Houston, R. Brent, Measuring and sorting cell populations expressing isospectral fluorescent proteins with different fluorescence lifetimes, PLoS One 9 (2014) e109940.
[23] J.W. Borst, M.A. Hink, A. van Hoek, A.J. Visser, Effects of refractive index and viscosity on fluorescence and anisotropy decays of enhanced cyan and yellow fluorescent proteins, J. Fluoresc. 15 (2005) 153–160.
[24] K.A. Walther, B. Papke, M.B. Sinn, K. Michel, A. Kinkhabwala, Precise measurement of protein interacting fractions with fluorescence lifetime imaging microscopy, Mol. BioSyst. 7 (2011) 322–336.
[25] D. Nicholls, S. Ferguson, BioenergeticsElseveier Store 2013.
[26] V. Wilkens, W. Kohl, K. Busch, Restricted diffusion of OXPHOS complexes in dynamic mitochondria delays their exchange between cristae and engenders a transitory mosaic distribution, J. Cell Sci. 126 (2013) 103–116.
[27] H. Schagger, K. Pfeiffer, Supercomplexes in the respiratory chains of yeast and mammalian mitochondria, EMBO J. 19 (2000) 1777–1783.
[28] R. Rossignol, R. Gilkerson, R. Aggeler, K. Yamagata, S.J. Remington, R.A. Capaldi, Energy substrate modulates mitochondrial structure and oxidative capacity in cancer cells, Cancer Res. 64 (2004) 985–993.
[29] A. Herms, M. Bosch, B.J. Reddy, N.L. Schieber, A. Fajardo, C. Ruperez, A. Fernandez-Vidal, C. Ferguson, C. Rentero, F. Tebar, C. Enrich, R.G. Parton, S.P. Gross, A. Pol, AMPK activation promotes lipid droplet dispersion on detyrosinated microtubules to increase mitochondrial fatty acid oxidation, Nat. Commun. 6 (2015) 7176.
[30] U. Lieberwirth, J. Arden-Jacob, K.H. Drexhage, D.P. Herten, R. Muller, M. Neumann, A. Schulz, S. Siebert, G. Sagner, S. Klingel, M. Sauer, J. Wolfrum, Multiplex dye DNA sequencing in capillary gel electrophoresis by diode laser-based time-resolved fluorescence detection, Anal. Chem. 70 (1998) 4771–4779.
[31] J. Enderlein, P.M. Goodwin, A. van Orden, W.P. Ambrose, R. Erdmann, R.A. Keller, A maximum likelihood estimator to distinguish single molecules by their fluorescence decay, Chem. Phys. Lett. 270 (1997) 464–470.
[32] Y. Yoon, E.W. Krueger, B.J. Oswald, M.A. McNiven, The mitochondrial protein hFis1 regulates mitochondrial fission in mammalian cells through an interaction with the dynamin-like protein DLP1, Mol. Cell. Biol. 23 (2003) 5409–5420.
[33] K. Yamano, R.J. Youle, PINK1 is degraded through the N-end rule pathway, Autophagy 9 (2013) 1758–1769.
[34] W. Lin, U.J. Kang, Characterization of PINK1 processing, stability, and subcellular localization, J. Neurochem. 106 (2008) 464–474.
[35] E. Deas, H. Plun-Favreau, S. Gandhi, H. Desmond, S. Kjaer, S.H. Loh, A.E. Renton, R.J. Harvey, A.J. Whitworth, L.M. Martins, A.Y. Abramov, N.W. Wood, PINK1 cleavage at position A103 by the mitochondrial protease PARL, Hum. Mol. Genet. 20 (2011) 867–879.
[36] S.M. Jin, M. Lazarou, C. Wang, L.A. Kane, D.P. Narendra, R.J. Youle, Mitochondrial membrane potential regulates PINK1 import and proteolytic destabilization by PARL, J. Cell Biol. 191 (2010) 933–942.
[37] L.A. Banaszynski, C.W. Liu, T.J. Wandless, Characterization of the FKBP·rapamycin·FRB ternary complex, J. Am. Chem. Soc. 127 (2005) 4715–4721.
[38] G. Miesenbock, D.A. De Angelis, J.E. Rothman, Visualizing secretion and synaptic transmission with pH-sensitive green fluorescent proteins, Nature 394 (1998) 192–195.
[39] C. Tregidgo, K. Suhling, Refractive index sensing using fluorescence lifetime imaging (FLIM), vol. 64422007 (pp. 64420 W–64420 W-64428).
[40] H.J. van Manen, P. Verkuijlen, P. Wittendorp, V. Subramaniam, T.K. van den Berg, D. Roos, C. Otto, Refractive index sensing of green fluorescent proteins in living cells using fluorescence lifetime imaging microscopy, Biophys. J. 94 (2008) L67–L69.
[41] A. Colbeau, J. Nachbaur, P.M. Vignais, Enzymic characterization and lipid composition of rat liver subcellular membranes, Biochim. Biophys. Acta 249 (1971) 462–492.
[42] A. Livigni, A. Scorziello, S. Agnese, A. Adornetto, A. Carlucci, C. Garbi, I. Castaldo, L. Annunziato, E.V. Avvedimento, A. Feliciello, Mitochondrial AKAP121 links cAMP and src signaling to oxidative metabolism, Mol. Biol. Cell 17 (2006) 263–271.
[43] I. Wittig, R. Carrozzo, F.M. Santorelli, H. Schagger, Supercomplexes and subcomplexes of mitochondrial oxidative phosphorylation, Biochim. Biophys. Acta 1757 (2006) 1066–1072.
[44] T. Althoff, D.J. Mills, J.L. Popot, W. Kuhlbrandt, Arrangement of electron transport chain components in bovine mitochondrial supercomplex I1III2IV1, EMBO J. 30 (2011) 4652–4664.
[45] E. Schafer, H. Seelert, N.H. Reifschneider, F. Krause, N.A. Dencher, J. Vonck, Architecture of active mammalian respiratory chain supercomplexes, J. Biol. Chem. 281 (2006) 15370–15375.
[46] T. Niehorster, A. Loschberger, I. Gregor, B. Kramer, H.J. Rahn, M. Patting, F. Koberling, J. Enderlein, M. Sauer, Multi-target spectrally resolved fluorescence lifetime imaging microscopy, Nature Methods, 2016.
[47] J.J. Lemasters, Variants of mitochondrial autophagy: types 1 and 2 mitophagy and micromitophagy (Type 3), Redox Biol. 2 (2014) 749–754.
[48] Y. Cotte, M.F. Toy, E. Shaffer, N. Pavillon, C. Depeursinge, Sub-Rayleigh resolution by phase imaging, Opt. Lett. 35 (2010) 2176–2178.
[49] B. Muster, W. Kohl, I. Wittig, V. Strecker, F. Joos, W. Haase, J. Bereiter-Hahn, K. Busch, Respiratory chain complexes in dynamic mitochondria display a patchy distribution in life cells, PLoS One 5 (2010) e11910.